International Journal of Hyperthermia

ISSN: 0265-6736 (Print) 1464-5157 (Online) Journal homepage: informahealthcare.com/journals/ihyt20

Controlled radio-frequency hyperthermia using an MR scanner and simultaneous monitoring of temperature and therapy response by ^{1}H, ^{23}Na and ^{31}P magnetic resonance spectroscopy in subcutaneously implanted 9L-gliosarcoma

Judy R. James, Yong Gao, Victor C. Soon, Stephen M. Topper, Andriy Babsky & Navin Bansal

To cite this article: Judy R. James, Yong Gao, Victor C. Soon, Stephen M. Topper, Andriy Babsky & Navin Bansal (2010) Controlled radio-frequency hyperthermia using an MR scanner and simultaneous monitoring of temperature and therapy response by ^{1}H, ^{23}Na and ^{31}P magnetic resonance spectroscopy in subcutaneously implanted 9L-gliosarcoma, International Journal of Hyperthermia, 26:1, 79-90, DOI: 10.3109/02656730903373509

To link to this article: https://doi.org/10.3109/02656730903373509

Int. J. Hyperthermia, February 2010; 26(1): 79–90

informa
healthcare

Controlled radio-frequency hyperthermia using an MR scanner and simultaneous monitoring of temperature and therapy response by ^{1}H, ^{23}Na and ^{31}P magnetic resonance spectroscopy in subcutaneously implanted 9L-gliosarcoma

JUDY R. JAMES[1,2], YONG GAO[1], VICTOR C. SOON[1], STEPHEN M. TOPPER[1], ANDRIY BABSKY[1], & NAVIN BANSAL[1,2]

[1]*Department of Radiology, Indiana University School of Medicine, Indianapolis, Indiana and* [2]*School of Health Sciences, Purdue University, West Lafayette, Indiana*

(Received 7 April 2009; Revised 22 September 2009; Accepted 27 September 2009)

Abstract

A magnetic resonance (MR) technique is developed to produce controlled radio-frequency (RF) hyperthermia (HT) in subcutaneously-implanted 9L-gliosarcoma in Fisher rats using an MR scanner and its components; the scanner is also simultaneously used to monitor the tumour temperature and the metabolic response of the tumour to the therapy. The method uses the ^{1}H chemical shift of thulium 1,4,7,10-tetraazacyclododecane-1,4,7,10-tetra-acetic acid ($TmDOTA^{-}$) to monitor temperature. The desired HT temperature is achieved and maintained using a feedback loop mechanism that uses a proportional-integral-derivative controller. The RF HT technique was able to heat the tumour from 33° to 45°C in ~10 min and was able to maintain the tumour temperature within ±0.2°C of the target temperature (45°C). Simultaneous monitoring of the metabolic changes with RF HT showed increases in total tissue and intracellular Na^{+} as measured by single-quantum and triple-quantum filtered ^{23}Na MR spectroscopy (MRS), respectively, and decreases in intra- and extracellular pH and cellular bioenergetics as measured by ^{31}P MRS. Monitoring of metabolic response in addition to the tumour temperature measurements may serve as a more reliable and early indicator of therapy response. In addition, such measurements during HT treatment will enhance our understanding of the tumour response mechanisms during HT, which may prove valuable in designing methods to improve therapeutic efficiency.

Keywords: *RF hyperthermia, MRI, sodium, pH, cellular energy*

Introduction

Radiofrequency (RF) hyperthermia (HT) has proved to be an adjuvant form of cancer treatment to radiotherapy and chemotherapy for treating some human cancers [1, 2]. In HT therapy, the temperature of the tumour is raised by a few degrees (~41–45°C) above the normal body temperature [3]. The effectiveness of HT is dependent on various factors such as tumour type and tissue characteristics, the temperature achieved during the treatment and the length of the HT treatment. One of the major concerns during HT is the need to maintain the tumour temperature at a desired level (41–45°C) with minimal thermal damage to vital normal tissues. The lack of proper heating and temperature monitoring has been a major obstacle in evaluating the efficacy of HT treatment in many previous studies [4]. Thus, there are continued efforts to develop optimal non-invasive techniques to deliver heat and to monitor the tumour temperature during the treatment in both experimental [5, 6] and clinical [7] HT studies.

The effects of HT on plasma membrane permeability and ionic exchange processes have been

Correspondence: Navin Bansal, PhD, Department of Radiology, Indiana University School of Medicine, 950 West Walnut Street, R2 E124, Indianapolis, IN 46202-5181, USA. Tel: (317) 278-0006. Fax: (317) 274-1067. E-mail: nbansal@iupui.edu

ISSN 0265–6736 print/ISSN 1464–5157 online
DOI: 10.3109/02656730903373509

suggested to play a key role in cellular damage and death from the treatment [8–11]. A trans-membrane sodium concentration (Na^+) gradient that is essential in maintaining cellular ion homeostasis for cell survival could be disrupted when heat is applied, therefore the effects of HT on total tissue (Na_t^+) and intra-cellular sodium (Na_i^+) may be useful for monitoring therapy response. Temperature can also influence pH considerably due to changes in energy metabolism. A decrease in the nucleoside-tri-phosphates (NTP), and an increase in inorganic phosphate (P_i) levels, as well as the intracellular pH (pH_i) shifting towards the acidic state, are some of the responses exhibited with HT treatment monitored using ^{31}P NMR [9, 12–15]. Monitoring cellular metabolic response during HT treatment may be more reliable in assessing therapy efficacy than monitoring temperature alone because different tumours and tumour regions may have different vulnerabilities to heat.

A magnetic resonance (MR) spectrometer that is equipped with RF systems to excite spins can enable an in-magnet HT application with simultaneous non-invasive temperature monitoring and control and to combine this RF HT technique with multi-nuclear MR measurements would allow simultaneous investigation of the metabolic and physiological effects of HT treatment on tumours [5, 6]. One goal in this work was to develop a robust non-invasive method for delivering in-magnet controlled RF HT to heat subcutaneously (sc) implanted tumours using the same RF volume coil as used for MR data collection, and incorporate this RF HT technique with ^{23}Na and ^{31}P MR spectroscopy (MRS) data collection. Another goal was to apply the developed controlled HT technique to monitor the effects of HT on Na_t^+ as measured by single-quantum (SQ) ^{23}Na MRS and Na_i^+ by triple-quantum filtered (TQF) ^{23}Na MRS, and cellular energy status (NTP/P_i) and intra- and extra-cellular pH (pH_i and pH_e, respectively) by ^{31}P MRS in sc implanted 9L-gliosarcoma in rats. The in-magnet RF HT technique controlled the heating using a proportional-integral-derivative (PID) feedback controller that was integrated into the MR system that adjusted the RF power level automatically to maintain the tumour temperature at a desired level during heating and MR data collection. Non-invasive temperature measurements based on the strong temperature dependence of the hyperfine chemical shift of a paramagnetic lanthanide complex 1,4,7,10-tetraazacyclodo-decane-1,4,7,10-tetra-acetic acid ($TmDOTA^-$) were used to measure the tumour temperature during RF heating [16–18]. The use of paramagnetic complexes for MR thermometry using Ni-N,N-diaminotroponiminate was first suggested by Jack Roberts at the California Institute of Technology in the 1960s (personal communication with J.D. Glickson, University of Pennsylvania, 2001). Among all the paramagnetic complexes proposed for MR thermometry, the macrocyclic complexes of thulium are most suitable for in vivo applications because of their high temperature sensitivity and high thermodynamic and kinetic stability [17].

Some of the advantages of the in-magnet controlled HT scheme include (1) better monitoring of the tumour temperature compared to invasive local temperature measurements with thermocouple or fibre-optic probes, (2) efficient control of the RF power to heat the tumour so that the tumour temperature can be locked at a desired value during the HT, and (3) simultaneous monitoring and assessment of the metabolic and physiological responses of the tumour during the HT treatment.

Methods

All MR experiments were performed on a Varian 9.4-T (Palo Alto, CA), 31 cm diameter horizontal bore scanner. A loop-gap resonator (diameter, 20 mm; depth, 18 mm) dual tuned to 400 MHz for ^1H, and either 106 MHz for ^{23}Na or 163 MHz for ^{31}P was used for MR data collection and RF heating. The homogeneity of RF heating produced by the coil was tested using a 2 mM $TmDOTA^-$ gel phantom that was heated from 17 to 27°C. 3D temperature maps computed from $TmDOTA^-$ showed that the standard deviation of the increase in temperature was 0.4°C across the whole image. Thus, the coil produced a homogenous RF field and heating in a homogeneous saline gel sample.

Development of in-magnet controlled RF HT with ^{23}Na and ^{31}P MR spectroscopy

Development and testing of in magnet controlled RF HT with ^{23}Na or ^{31}P MRS data collection was performed on a 2 mL glass vial containing 2 mM $TmDOTA^-$, 10 mM sodium phosphate (Na_2HPO_4) and 0.9% sodium chloride (NaCl) in 6% agarose gel.

The temperature of the sample was calculated from the chemical shift of H_6 resonance in $TmDOTA^-$. ^1H spectra from $TmDOTA^-$ were acquired at 400 MHz using a 400 μs sinc-shaped 90° excitation pulse over a spectral width of 100 kHz. The Chemical Shift Selective (CHESS) technique [19] was used to suppress the unwanted water signal. SQ and TQF ^{23}Na spectra were collected at 106 MHz. A pulse-acquire sequence with 100 ms pre-delay (pd), 90° excitation pulse width (pw) of 160 μs, 5 kHz spectral width (sw), and 1000 number of data points (np) was used. TQF ^{23}Na spectra were acquired with the following pulse sequence: $90° - \tau/2 - 180° - \tau/2 - 90° - \delta - 90°$ – acquisition. The preparation time (τ)

was 10 ms, and the evolution time (δ) was kept at a minimum (10 μs) to allow RF phase change and avoid signal loss due to TQ relaxation. A 48-step phase-cycling scheme was used to select the TQF signal [20]. All other parameters were similar as used for SQ ^{23}Na data collection. The data collection time for a SQ ^{23}Na spectrum with 32 signal averages was 13 s and that for a TQF ^{23}Na spectrum with 384 signal averages was 84 s. ^{31}P MRS data were collected at 165 MHz using a pulse-acquire sequence and the following parameters: pd = 1 s, flip angle = 60°, pw = 100 μs, sw = 20 kHz and np = 4000. The total data collection time for each ^{31}P spectrum with 64 signal averages was 71 s.

The in-magnet controlled RF HT procedure was developed and optimised for ^{23}Na and ^{31}P experiments separately. Sets of consecutive ^{1}H and ^{23}Na spectra or ^{1}H and ^{31}P spectra were collected continuously during a typical experiment. After collecting a set of baseline spectra, the decoupler power was turned on at 400 MHz during ^{23}Na or ^{31}P data collection for RF heating. The temperature of the sample was controlled by adjusting the decoupler power level using a PID controller. The controller used a feedback loop mechanism to adjust the RF power, $u(t)$, based on the error, $e(t)$, between the target temperature and the current sample temperature using the following equation:

$$u(t+1) = u(t) + K_p e(t) + K_d \frac{\mathrm{d}e(t)}{\mathrm{d}t} + K_i \int e(t)\mathrm{d}t \quad (1)$$

where, K_p, K_i and K_d are proportional, integral and derivative constants, respectively. The controller was optimised by simulations using Simulink, Matlab 7.0 (Math Works, Natick, MA). A flow chart of the simulation program is shown in Figure 1.

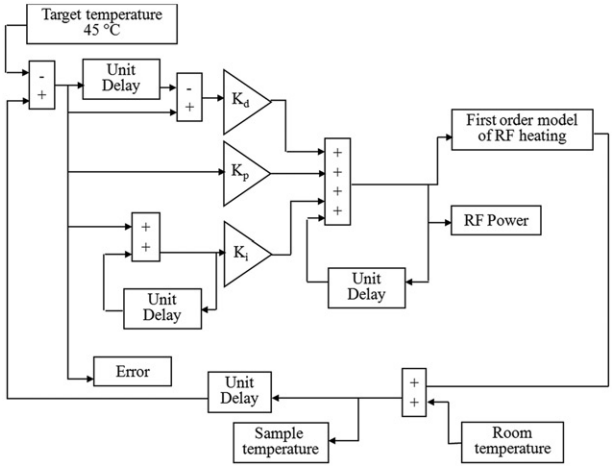

Figure 1. A flow chart of a PID temperature controller simulated using Simulink, Matlab. The simulation program was used to optimise the controller constants, K_d, K_p and K_i using a first order model of RF heating.

A first-order model of RF heating was used to describe the heating produced by RF irradiation. In this model the sample temperature, T_t, after RF irradiation at a constant power level P for time t is given by

$$T_t = (A \cdot P - T_0) \times [1 - \exp(-t \cdot k)] + T_0, \quad (2)$$

where T_0 is the initial temperature, and A and k are constants that depend on the experimental set-up. The term '$A \cdot P$' is equal to the steady-state temperature in the presence of long-term constant RF power irradiation. The values of A and k for RF HT with ^{23}Na and ^{31}P data collection were determined from open-loop curves. These curves were obtained by irradiating the phantom at different constant RF power levels. A set of open-loop curves for RF HT experiments with consecutive SQ and TQF ^{23}Na data collection is shown in Figure 2. The values of A and k were calculated by curve-fitting to Equation 2 and incorporated in the computer simulations. Optimal values for K_p, K_i and K_d were determined using the following criteria: (1) a rise time of >10–15 min to reach the target temperature, (2) a maximum overshoot of 0.5°C, and (3) a maximum settling time of 5 min after achieving the target temperature. The optimal values for the PID constants were chosen after investigating effects on temperature control with the target temperature set at 45°C using the simulation program.

After optimising the PID controller in computer simulations, the controller was implemented on the

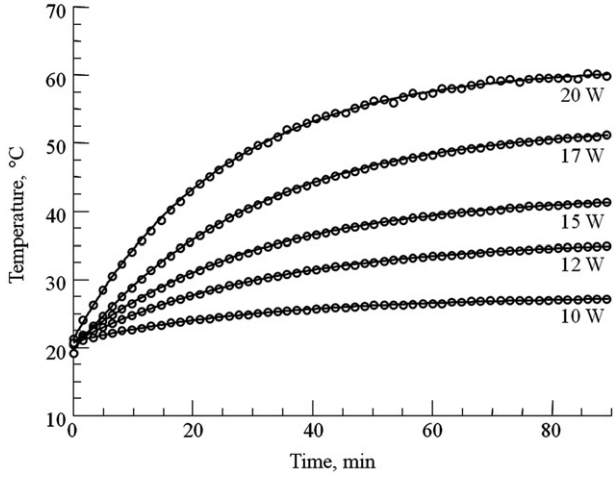

Figure 2. Open-loop temperature curves for SQ and TQF ^{23}Na experiments. The curves were obtained by irradiating the phantom with different constant RF power levels at 400 MHz during SQ and TQF ^{23}Na data collection. The temperature was monitored from the ^{1}H chemical shift of TmDOTA^{-}. The constant RF power (in W) for each curve is shown on right. These curves were fitted to Equation 2 and used to model the RF heating for simulating the PID controller.

Varian MR scanner and tested using the same phantom and dual tuned volume coil as used for obtaining the open-loop curves. After collecting a set of baseline ^{1}H and ^{23}Na spectra or ^{1}H and ^{31}P spectra, the RF power was turned on to heat the sample to the 45°C target temperature. The RF power was varied with the PID controller between 0 and 20 W while continuously collecting MRS data.

In vivo application of in-magnet controlled RF HT with ^{23}Na or ^{31}P MR spectroscopy

The in-magnet controlled RF HT technique combined with the MRS data collection was applied to investigate the effects of HT treatment (45°C for 30 min after tumour temperature reached 45°C) on sc-implanted 9L-gliosarcoma. Tumour Na_t^+ and Na_i^+ levels were measured by SQ and TQF ^{23}Na MRS, respectively, in one set of experiments, and cellular energy status (NTP/P_i), pH_i and pH_e were measured by ^{31}P MRS in another set of experiments.

Tumour model

9L-gliosarcoma cells were cultured with Dulbecco's modified Eagle's medium with 4 mM L-glutamine adjusted to contain 1.5 g/L sodium bicarbonate and 4.5 g/L glucose supplemented with 10% foetal bovine serum (ATCC, Manassas, VA). Approximately 4×10^6 cells in 0.1 mL phosphate buffer solution were injected sc into the right or left leg of male Fisher rats that were 6 weeks of age (70–110 g, $n = 6$). The tumours were allowed to grow to ~2 cm^3 over 20–25 days prior to MR experiments.

Animal preparation

The animal experiments were reviewed and approved by the institution's Animal Care and Use Committee. Rats were anaesthetised by inhalation of 1–2% isofluorane in 100% oxygen or medical air delivered through a face mask. The animal was positioned on a plastic cradle over a pneumatic respiration sensor (SA Instruments, Stony Brook, NY) for monitoring respiration during the MR experiments. The tumour was placed inside the dual tuned slotted tube resonator as shown in Figure 3. The whole set up with the cradle was then positioned inside the horizontal bore magnet. Warm air was blown into the magnet bore with a commercial hair-dryer (World Dreyer, Berkley, IL) to help maintain the animal core body temperature at ~35–36°C, which was monitored with a rectal fibre-optic probe (FOP) (FISO Technologies, Quebec, Canada). To monitor the surrounding temperature, an external FOP was placed near the tumour but without touching the tumour.

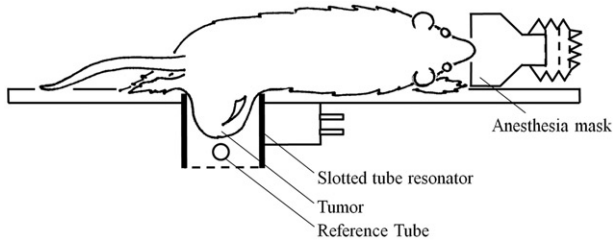

Figure 3. Schematic representation of the placement of the sc implanted 9L-gliosarcoma tumour into the dual tuned slotted tube resonator with an external reference placed near the tumour inside the coil.

In vivo SQ and TQF ^{23}Na MRS experiments

A group of five tumour-bearing rats were used for ^{23}Na MRS experiments. A 3–4 mL solution containing 100 mM $TmDOTA^-$ was injected through the jugular vein ~10 min before baseline MR data collection. A 1 mL vial containing 500 mM NaCl and 2.5 mM thulium-1,4,7,10-tetraazacyclododecane1,4,7,10-tetrakis-methylenephosphonate ($TmDOTP^{5-}$) in 10% agarose gel was placed near the tumour inside the dual tuned ^{1}H /^{23}Na coil and used as a SQ and TQF ^{23}Na integrated resonance intensity reference. $TmDOTP^{5-}$ was used to shift the reference ^{23}Na signal away from the tumour ^{23}Na signal. Agarose was used to generate a TQF ^{23}Na signal from the reference. SQ and TQF ^{23}Na spectra were collected using the same pulse sequences and parameters as used in the phantom experiments.

In vivo ^{31}P MRS experiments

A separate group of six tumour-bearing rats were used for ^{31}P MRS experiments. A solution containing 75 mM 3-aminopropylphosphonate (3-APP) and 100 mM TmDOTA- was infused through the jugular vein ~10 min prior to MRS experiments. ^{31}P signal from 3-APP was used for monitoring the pH_e [21]. A 1 mL vial containing 100 mM methyl-phosphonic acid (MPA) was placed inside the dual tuned $^{1}H/^{31}P$ coil and used as a ^{31}P external integrated intensity reference. ^{31}P spectra were also collected using the same parameters as used in the phantom experiments.

Protocol

The protocols for ^{23}Na and ^{31}P MR data collection during in-magnet controlled RF HT experiments are shown in Figure 4A and B. After baseline data collection, the RF power was turned on at 400 MHz during ^{23}Na or ^{31}P data collection. The target temperature was set to 45°C and the RF power was allowed to be varied by the PID controller. The RF heating was turned off after 30 min of irradiation and

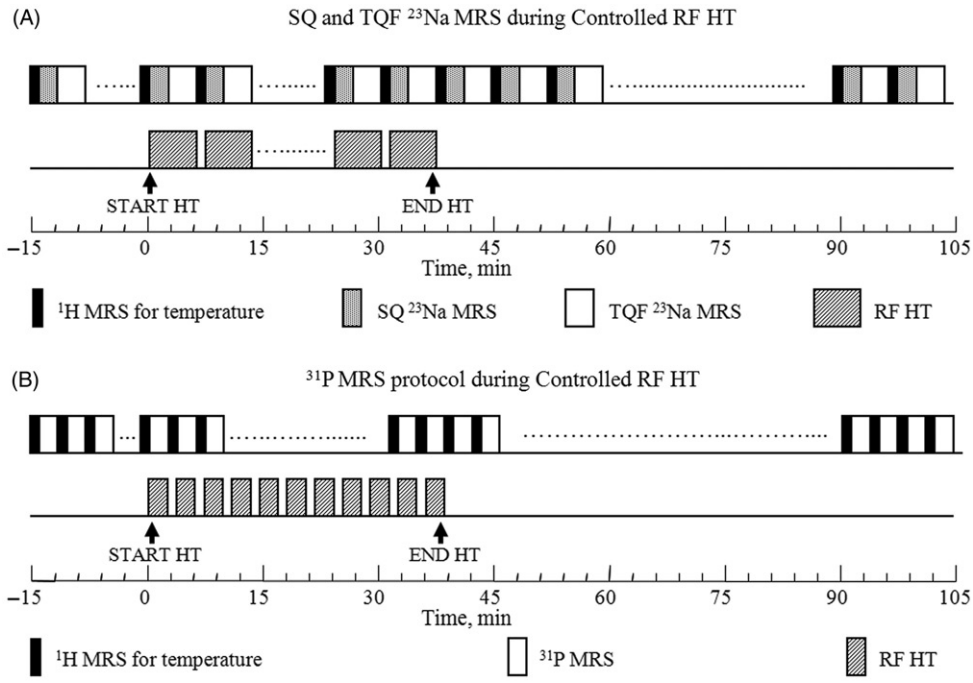

Figure 4. Experimental protocols for (A) SQ and TQF ^{23}Na and (B) ^{31}P MRS data collection during in-magnet controlled RF HT. Separate groups of 9L-gliosarcoma-bearing rats ($n = 5$) were examined by ^{23}Na and ^{31}P MRS experiments. After collecting eight sets of baseline ^{1}H and ^{23}Na or ^{31}P data, the RF HT was turned on and the tumour was allowed to reach 45°C while continuing the multi-nuclear data acquisition. The RF irradiation was turned off after 30 min of controlled HT at 45°C. The MR data collection was continued for an additional one hour during which time the tumour returned back to the baseline temperature.

the tumour temperature was allowed to return to the baseline temperature.

Data analysis and statistics

All MRS data was analysed using NMR Utility Transform Software (NUTS-Acorn NMR, Livermore, CA). The time-domain data were baseline corrected and multiplied by a single exponential corresponding to 400 Hz line-broadening for ^{1}H free-induction decay (FID), 10 Hz for SQ ^{23}Na FID, and 25 Hz for TQF ^{23}Na and ^{31}P FIDs before being Fourier transformed. Four sets of ^{31}P spectra were added together to improve signal-to-noise ratio and quantification. The various integrated resonance intensity areas in SQ and TQF ^{23}Na spectra and ^{31}P spectra were determined by integration. Cellular energy status was evaluated from the βNTP to P_i integrated resonance intensity ratios. βNTP signal was chosen since it does not contain contribution from adenosine diphosphates.

Temperature (T_{MRS}) was calculated from the ^{1}H chemical shift of $TmDOTA^{-}$ using the following relation:

$$T_{MRS} = \frac{F + C_0}{C_1} \tag{3}$$

where F is the chemical shift (in ppm) of the H_6 signal from $TmDOTA^{-}$ referenced to water at 4.7 ppm. $C_0 = 121.5$ ppm and $C_1 = 0.35$ ppm/°C are the zero and first order temperature calibration constants, respectively [16].

The heating and cooling time constants from the tumour temperature curve were estimated by curve fitting to exponential equations using PSI-Plot (Poly Software International, Pearl River, NY). The thermal dose at 43°C (tdm_{43}) in minutes was calculated from the time interval, Δt, initial temperature, T_0, and the average temperature, T_{av}, during Δt [22].

$$tdm_{43} = \frac{1}{43 - T_0} \sum_{t=0}^{\text{final}} (T_{av}(t) - T_0)\Delta t \tag{4}$$

Tumour pH_i was estimated from the chemical shift of P_i signal referenced to the αNTP signal in ^{31}P spectra using the relation [23].

$$pH_i = \frac{1979.5}{T + 273} - 5.4409 + 0.018567(T + 273) + \log\left(\frac{\delta_{(P_i - \alpha ATP)} - 10.72 + 0.003579T}{13.18 + 0.00188T - \delta_{P_i - \alpha ATP)}}\right) \tag{5}$$

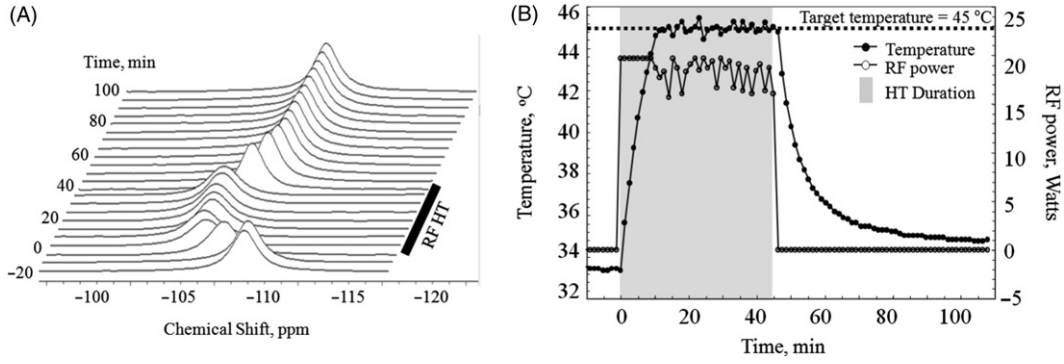

Figure 5. (A) Stacked plot of representative in vivo ^{1}H spectra from H_6 of TmDOTA$^-$ from sc implanted 9L-gliosarcoma during the controlled RF HT experiment. The chemical shift scale is referenced to the water resonance at 4.7 ppm. As tumour temperature was increased by RF heating, the ^{1}H signal shifted to the left. When the RF was turned off, the signal shifted back to the original position. (B) A plot of tumour temperature calculated from the chemical shift of TmDOTA$^-$ and RF power level during the 45°C HT experiment. The PID controller modulated the RF power for heating such that the tumour temperature remained at 45 ± 0.2°C.

where T is temperature in °C. Tumour pH_e was calculated from the shift of the 3-APP signal referenced to αNTP [21].

$$pH_e = 6.91 - \log\left(\frac{\delta_{(3APP-\alpha ATP)} - 31.11}{34.3 - \delta_{(3APP-\alpha ATP)}}\right) \quad (6)$$

Tumour temperatures, pH_i and pH_e are represented as mean ± standard error of mean (SEM). Na_i^+, (Na_t^+) and βNTP/P_i are presented relative to the baseline values set to 100. Statistical analysis of the data was performed by Student's t-test. A p-value ≤ 0.05 was considered significant compared to the baseline (pre-HT) data set.

Results

In-magnet controlled HT technique

The optimisation of PID controller constants with computer simulation using the mono exponential heating model yielded the optimum values of $K_p = 1000$, $K_d = 1000$, and $K_i = 0$. With these controller constants, the RF HT technique was able to heat the phantom from 30 to 45°C in ~10 min and then maintain the temperature at 45 ± 0.05°C.

A stacked plot of in vivo ^{1}H NMR spectra of TmDOTA$^-$ from a sc implanted tumour showing the frequency shift of the H_6 resonance before, during and after controlled RF HT treatment is shown in Figure 5A.

At baseline, the ^{1}H signal resonates at ~109 ppm, which corresponds to 33.7°C. As the tumour temperature was increased by RF irradiation, the ^{1}H signal shifted to the left. During the temperature stabilisation phase, the signal frequency remained relatively stable at 105.7 ppm, which corresponds to 45°C. When the RF power was turned off, the tumour temperature decreased and the H_6 signal shifted back close to its baseline position. A temperature plot for a sc-implanted tumour during a typical controlled RF HT experiment with SQ and TQF MRS data collection is shown in Figure 5B. Application of the in-magnet controlled RF HT technique raised the tumour temperature from 33.7 to 45°C in about 10–15 min with an average time constant of 10 ± 2 min to reach the target temperature. After the target temperature was achieved, the RF heating power was adjusted and modulated automatically as per Equation 1 to maintain the tumour temperature at ~45°C. The RF power varied between 15 and 20 W during the heating. While the rise time for heating the tumour was slightly longer than that for the phantom due to heat dissipation by blood, the PID controller was able to maintain the tumour temperature at 44.9 ± 0.2°C. After 30 min of HT, the RF power was turned off and the tumour returned to its baseline temperature (33.4°C) in ~1 h. The average cooling time constant was estimated to be 16.9 ± 3.4 min. Integration of these temperature plots yielded an average tdm_{43} of 57 ± 2 min (Equation 4) for all ^{23}Na and ^{31}P experiments. The rectal temperature remained at 35 ± 1°C throughout the experiment including during the HT treatment.

Effects of in-magnet HT on SQ and TQF ^{23}NaMRS:

Representative in vivo SQ and TQF ^{23}Na spectrum from a 9L-gliosarcoma collected before, 30 min during and 40 min after controlled RF HT treatment, are shown in Figure 6. Each of the SQ and TQF ^{23}Na spectrum shows two resonances, one from the tumour at 0 ppm and another from the reference containing 2.5 mM TmDOTP^{5-} at ~2 ppm. As HT was administered to the 9L-gliosarcoma, increases in both the SQ and TQF ^{23}Na signal areas (SA) were observed. Relative changes in SQ and TQF ^{23}Na SA

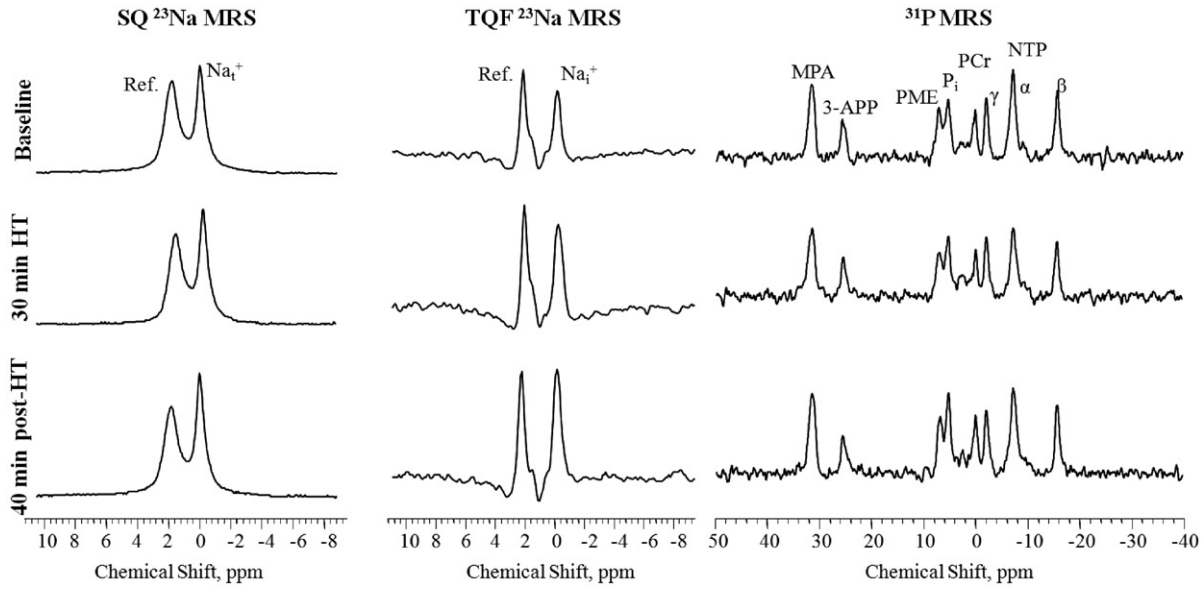

Figure 6. Representative in vivo SQ (left), TQF (middle) ^{23}Na and ^{31}P spectra (right) from sc-implanted 9L-gliosarcoma before (top), at the end of 30 min controlled HT (middle), and after 40 min of HT treatment. SQ and TQF ^{23}Na spectra show peaks from the tumour and the reference containing $TmDOTP^{5-}$. The chemical shift scale is referenced to tissue ^{23}Na resonance at 0 ppm. ^{31}P spectra show the different metabolite resonances from the tumour, the external reference, MPA, and the pH_e probe, 3-APP. The PCr resonance is assigned as 0 ppm.

averaged for all the tumours ($n = 5$) are shown in Figure 7A. Controlled RF HT produced a gradual increase in both SQ and TQF ^{23}Na SA. These changes in SQ ^{23}Na spectra reflects changes in tumour Na_t^+ and those in TQF ^{23}Na spectra reflects changes in tumour Na_i^+ [20]. The HT treatment produced a 30–40% ($p \leq 0.05$) irreversible increase in TQF ^{23}Na SA compared to a reversible 12% increase ($p \leq 0.05$) in SQ ^{23}Na SA. TQF ^{23}Na SA continued to increase even after the heating was stopped and tumour temperature returned to the baseline value.

Effects of in-magnet HT on ^{31}P MRS

Representative in vivo ^{31}P spectra collected from a tumour before, 30 min during, and 40 min after the controlled RF HT treatment are shown in Figure 6. Each of the ^{31}P spectrum shows three NTP resonances from α-, β- and γ-phosphate groups, a phosphocreatine (PCr) resonance, a P_i resonance, and a phosphomonoester (PME) resonance from the 9L-gliosarcoma. ^{31}P resonances from the external reference that contained MPA and the pH_e probe, 3-APP, that was infused prior to start of the experiment can also be observed at 31.8 and 24.91 ppm, respectively. The effects of HT on changes in pH_i and pH_e calculated from Equations 5 and 6, and the relative changes in βNTP/P_i peak areas averaged for all the tumours ($n = 6$) are shown in Figure 7B and C. The tumour pH_i and pH_e were 7.08 ± 0.1 and 6.89 ± 0.05 units, respectively, prior to HT. This trans-membrane pH gradient in the tumour is opposite to that seen in normal tissues which have a pH_i of ~7.1 and a pH_e of 7.3–7.4 [24]. As the tumour temperature increased, pH_i decreased by ~0.2 units, from 7.04 ± 0.05 to 6.89 ± 0.03 ($p \leq 0.05$) but then returned back to its baseline value 15 min after RF power for HT was turned off. pH_i remained at the baseline value during the remaining experimental period including the post-HT period. pH_e decreased by ~0.17 units from 6.92 ± 0.04 to 6.75 ± 0.04 ($p \leq 0.05$) with the onset of HT. It is interesting to note that the decrease in pH_e occurred 10–12 min after the decrease in pH_i. pH_e remained acidic throughout the HT treatment but then gradually returned back to the baseline value (6.9 ± 0.1) when the heating was terminated. The changes in relative cellular energy status as measured by βNTP/P_i SA ratios before, during and after HT are shown in Figure 7C. When HT was applied, βNTP/P_i decreased by ~40% ($p \leq 0.05$) during HT and remained depressed after HT. Changes in NTP and P_i were also measured relative to the external reference, MPA, placed beside the tumour inside the coil. βNTP/MPA showed an ~18% decrease accompanied by a simultaneous ~30% increase in the P_i/MPA compared to their respective baseline levels at the end of HT treatment (data not shown).

Discussion

The in-magnet controlled RF HT technique presented here has several important characteristics. It uses the same RF coil and MR hardware system for

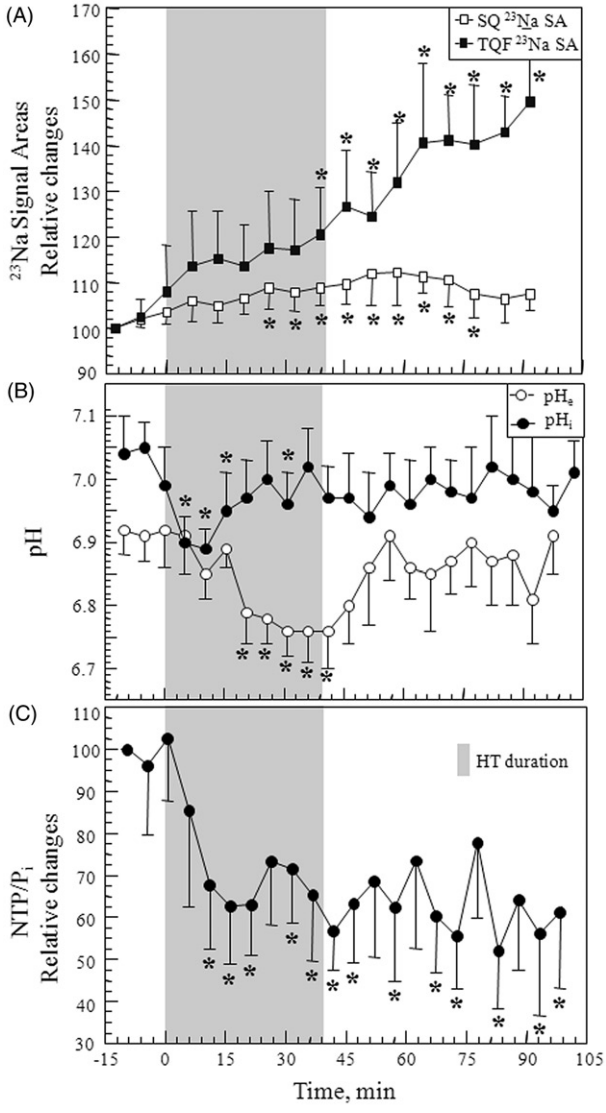

Figure 7. Effects of 45°C HT on (A) SQ and TQF ^{23}Na signal areas ($n=5$), (B) pH_i and pH_e ($n=6$), and (C) NTP/P_i ($n=6$) in sc implanted 9L-gliosarcoma (mean ± SEM). SQ and TQF ^{23}Na signal areas and NTP/P_i baseline levels were normalised to 100. $^{\star}p \leq 0.05$ versus pre-HT baseline data.

exciting the nuclear spins. It monitors the tumour temperature from the ^{1}H chemical shift of TmDOTA, which is 50–100 times more sensitive to temperature than water ^{1}H shifts [17]. It maintains the tumour temperature within ±0.2°C of the target temperature with an integrated PID controller. Finally, this technique acquires SQ and TQF ^{23}Na or ^{31}P MRS data consecutively with ^{1}H MRS data collection during controlled RF HT for monitoring the metabolic and physiological effects of the treatment.

During MR studies RF can cause significant heating problems in tissues if the specific absorption rate (SAR) limits are exceeded [25]. This disadvantage of RF heat to normal tissues has been exploited and utilised to deliver controlled RF HT treatment to sc-implanted tumour in the rat. The frequency of RF generally used for heating tumours in humans is 2–4 MHz because the wavelengths associated with this frequency range are considerably longer than the dimensions of parts of the human body [26]. The RF frequency of 400 MHz used in the present study was adequate to produce relatively uniform heating because animal tumours are only 1–2 cm in diameter. RF irradiation can heat up tumours more easily than normal tissues because tumours have poor vasculature and compromised blood flow. In addition, the equation, $W = 0.5 \times \sigma \times E^2$, where σ is the conductivity of the material and E is the electric field produced in the tissue, predicts that RF heating produces higher increases in temperature with increasing ionic strength [27]. In general, tumours have higher sodium concentration compared to normal tissue due to a lager relative extracellular space (rECS) and high Na_i^+ concentration. The larger extracellular space results from inefficient cell packing and the high Na_i^+ concentrations results from abnormal metabolism and ion physiology [28]. Because of their high sodium concentration and high ionic conductivity, tumours can be heated more easily than normal tissues by RF irradiation. The higher ionic conductivity in tumours has been proved by the fact that Na^+ content in the tumours was measured to be three times more than that in the normal cells [29] as measured by NMR and flame photometry whereas the K^+ concentration was either similar or 1.2 times reduced in tumours when compared to normal tissues [30]. Furthermore, RF exposure does not increase the temperature of the sc fat layer because of the low conductivity of fat, compared to the sc-implanted tumour.

The use of the same MR spectrometer with its components for RF heating as well as to excite spins to perform MR data collection was first proposed by Naruse et al. [13]. In their study, they delivered RF HT to a sc-implanted tumour model in rat by applying continuous RF power to a surface coil. The two major drawbacks of the previous study were that it did not make any effort to control the tumour temperature during the treatment, and the use of a surface coil produced very heterogeneous intratumoural temperature during RF HT. In contrast, the loop-gap resonator used in the present study provided a relatively homogeneous RF field throughout the tumour, which did not extend significantly into the normal tissue.

Jayasundar et al. presented another experimental set-up for the use of an MR spectrometer as an RF HT applicator for rodent tumour models [6]. In their set-up, a thermocouple was used to monitor and

maintain the tumour temperature using a feedback system. However, the use of a thermocouple has several disadvantages. It allows temperature measurements from only one region in the tissue, and insertion of the probe into tissue alters the physiology and thermal characteristics of the tissue. In addition, if proper care is not taken, the metallic conductors of a thermocouple can interfere with MR data collection, and the presence of a strong RF field in pulse spectroscopy could alter the output of the invasive temperature monitoring device. The proposed use of $TmDOTA^{-}$ as an MR thermometer during RF HT does not suffer from these disadvantages.

More recently, Bezabeh et al. [5] implemented a dual antenna-coil methodology to administer 'in-magnet' RF HT with a separate 4 MHz RF amplifier and simultaneously collected ^{31}P MR spectra during HT treatment. A number of precautions such as band-pass filters and orthogonal RF coil arrangements were necessary to avoid interference between RF heating and MR data collection. In addition, FOPs were inserted in the sc-implanted tumour to monitor tumour temperature and control the RF power for heating with a feedback mechanism.

The use of an MR system for simultaneously administering controlled HT and collecting temperature and metabolic data developed here is an ideal set-up for sc-implanted tumours in rats and mice. Since RF for both heating and MR experiments are controlled by the same computer, they can be easily synchronised to avoid interference from each other and to deliver controlled HT. The PID controller used in the present study was able to achieve and maintain the desired tumour temperature within $\pm 0.2^{\circ}C$ during RF HT without the use of any additional electronics. Such a tight control over the temperature was achieved by optimising the controller with computer simulations and phantom experiments. Since K_p, K_i and K_d are dependent on each other, a change in one of these variables affects the functioning of the others. Our simulation with different combinations of K_p, K_i and K_d showed that deviations in the values reported resulted in a longer rise-time (greater than 15–20 min), larger overshoot (greater than 1 or $2^{\circ}C$) and/or more steady-state errors. Optimisation of K_p aided in reducing both the rise-time and steady-state errors but did not eliminate them. Optimisation of K_d had the greatest effect on increasing the stability of the system by reducing the overshoot, allowing for a very short settling time and almost eliminating the steady-state errors. The integral constant was set to zero because a positive value for the constant produced a large overshoot (5–$10^{\circ}C$) and a longer settling time. The rise time of the PID controller could be further reduced by using a higher maximum RF power level. The present study used a maximum of ~20 W power to avoid damage to the RF coil. Even though the PID controller coefficients were optimised using Matlab simulation with the first order model for the phantom, the controller was still able to perform well on the sc-implanted tumours in rats without any changes needed to the PID coefficients. This shows that the PID controller is robust and is able to account for any model deviations from the ideal phantom such as animal tumours, which will typically have differences in mass, perfusion, and conductive properties, etc.

The tumour temperature was monitored from the ^{1}H frequency shift of $TmDOTA^{-}$, which is 35 times more sensitive to temperature (temperature co-efficient (C_T) = 0.35 ppm/$^{\circ}C$) than the intrinsic water ^{1}H signal (C_T = 0.01 ppm/$^{\circ}C$) [31]. ^{1}H chemical shift of $TmDOTA^{-}$ is ~100 ppm to lower frequency for the ^{1}H resonance of water, allowing selective excitation of the complex with the CHESS water suppression technique. Moreover, the temperature dependence of ^{1}H shift of this complex is insensitive to tissue pH, calcium ion concentration, or other macromolecules and ions [16]. All the animals in the study tolerated the injected 3–4 mL solution containing 100 mM $TmDOTA^{-}$ well and did not show any acute adverse effects. Normal breathing patterns were observed before, during and after the injection of $TmDOTA^{-}$. The long-term effects of $TmDOTA^{-}$ on renal function or other measures of toxicity were not evaluated in the present study but the behaviour of $TmDOTA^{-}$ is expected to be similar to that of $GdDOTA^{-}$ because of the close chemical relationship between the two complexes [17]. Use of $TmDOTA^{-}$ in combination with water signal allows for in vivo absolute temperature measurements which is not possible with water signal alone [32]. These characteristics make $TmDOTA^{-}$ a suitable non-invasive probe for in vivo monitoring of tumour temperature during HT treatment.

The ^{1}H line-width of $TmDOTA^{-}$ signal increased from 450–475 Hz at baseline to ~650 Hz when the tumour first achieved an average temperature of $45^{\circ}C$. The line width reduced to ~535 Hz at the end of HT and then returned to ~450 Hz when the tumour temperature returned to the baseline value. If we assume that these changes in ^{1}H line width are dominated by the spatial temperature distribution, then the 200 Hz increase in the line width when the tumour first achieved $45^{\circ}C$, corresponds to a tumour temperature heterogeneity of ~$1.4^{\circ}C$. Thus, the slotted tube resonator produced relatively homogeneous RF heating despite the possible variations in the perfusion and ionic conductivity within the tumour.

In vivo ^{23}Na and ^{31}P MRS measurements were performed in this study to monitor the therapy responses of the tumour during HT treatment.

Monitoring the biological response of tumours simultaneously with HT treatment may be more accurate than temperature measurements alone because different tumours may have different vulnerabilities to temperature. For example, it is well known that tumours are more sensitive to heating in an acidic environment [33]. Thus, for a given thermal dose, an acidic tumour would be more effectively treated than a tumour at a higher pH. Monitoring the temperature alone in such a case would be less predictive of therapy response than monitoring the metabolic response.

A number of reports have proposed that the plasma membrane is a critical target for HT-induced cell death [9–11]. Proper functioning of the plasma membrane with respect to permeability and transport processes across the membrane is vital to living cells. Active transport systems create and maintain ionic gradients. Thus, heat can produce significant alterations in trans-membrane sodium and pH gradients [8, 9, 14, 15]. These ion gradients can also be affected by disruption of cellular energy metabolism during HT treatment [9, 12].

^{23}Na MRS provides a convenient, relatively sensitive, and non-destructive method for monitoring Na_t^+ in tissue. However, ^{23}Na signals from Na_i^+ and Na_e^+ resonate at the same frequency because Na^+ exists in only one chemical form in tissue. This study used TQF ^{23}Na MRS to monitor changes in Na_i^+ selectively. The TQF ^{23}Na MRS technique depends only on the difference in the relaxation properties of Na_i^+ and Na_e^+ and does not produce any physiological perturbation to the biological system. Previous studies demonstrate that although a significant Na_e^+ signal contributes to the TQF signal from 9L-gliosarcoma and other tissue, this contribution is small compared to Na_i^+ signal. In addition TQF Na_e^+ signal is relatively insensitive to changes in Na_e^+ content [20]. Thus, the TQF ^{23}Na signal can be used to monitor changes inNa_i^+.

The SQ and TQF ^{23}Na MRS data presented here show that HT induced increases in both Na_t^+ and Na_i^+. An increase in Na_t^+ could result from an increase in rECS and/or an increase in Na_i^+. Although, rECS was not measured in the present study, changes in vascular permeability at 45°C can cause extracellular oedema and increase rECS [34]. An irreversible increase in Na_i^+ was clearly evident from the TQF ^{23}Na data. These findings are consistent with the in vitro results obtained with HT on superfused RIF-1 cells [9]. Exposure to elevated temperature could increase the fluidity of the plasma membrane, which in turn could increase the simple diffusion of Na^+ ions into the cells along the concentration gradient. Temperature could also alter the activity of ion transport proteins directly and hence change Na_i^+. Previous studies have demonstrated that cytotoxic temperatures inhibit Na^+/K^+-adenosine triphosphate(ATP)ase [35]. However, the thermosensitivity of this ion pump seems to depend on cell type because other studies showed no impairment [36] or even an increase in the Na^+-pump activity during HT [10].

In vivo ^{31}P NMR experiments show that HT produced an irreversible 40% decrease in NTP/P_i at the end of HT whereas pH_i and pH_e showed reversible decreases by ~0.2 pH units during HT. These changes in cellular energy status and pH in the 9L gliosarcoma model are smaller compared to that reported for sc-implanted RIF-1 tumours [5, 12, 13, 15] perhaps because of differences in the two tumour models. Previous HT studies on sc-implanted C6 glioma (13) and perfused gliosarcoma cells (11) also showed small changes in tumour pH (0.2 units) as reported here. The in vivo C6 glioma study reported that the NTP levels are decreased 30 minutes, 3 hours and 7 days after HT treatment but did not provide any quantitative changes. The HT induced decrease in cellular energetics in the 9L gliosarcoma in the present study remained depressed up to 60 minutes after HT. It is likely that the cellular energetics would deteriorate further with time, which could explain the smaller decrease in NTP/P_i reported here compared to the previous studies in which the ^{31}P MRS measurements were performed at later times after HT [5, 12, 13, 15]. The decrease in cellular energy status with HT could result from heat-induced vascular damage at 45°C HT, causing a decrease in tumour oxygen supply and shifting the tumour cell metabolism from oxidative phosphorylation to glycolysis [37]. A small decrease in oxidative metabolism can produce a dramatic decrease in cellular NTP levels because complete oxidation of glucose produces 38 NTP molecules, while glycolysis only produces 2 NTP per glucose. The compromised cellular energy status may be partially responsible for the observed increase in Na_i^+ from the reduced activity of energy-requiring Na^+/K^+-ATPase [9].

An interesting trend was observed in the changes in tumour pH_i and pH_e with HT treatment. The tumour pH_i initially decreased but then recovered with a simultaneous decrease in pH_e during the HT treatment. pH_e returned back to its baseline value after the HT administration. The exact mechanism of the initial pH_i decrease is not clear but it may result from increased glycolysis and hence lactic acid production. The recovery of pH_i with a simultaneous decrease in pH_e during HT suggests activation of membrane H^+ transporters to maintain pH_i homeostasis. Strict regulation of pH_i is essential for cellular metabolism and proliferation. The amiloride sensitive Na^+/H^+ antiporter has been suggested to play an important role in maintenance of pH_i [8, 9].

Proton removal by the Na^+/H^+ exchanger is driven by the free energy of the Na^+ gradient. It has been previously shown that in perfused RIF-1 cells, inhibition of Na^+/H^+ with 5-(N-ethyl-N-isopropyl) amiloride during HT treatment attenuates the therapy-induced increase in Na_i^+ [8]. Thus the observed initial decrease in pH_i followed by its recovery with simultaneous decrease in pH_e and the increase in Na_i^+ during HT may all be interrelated and demonstrate a mechanism that protects tumour cells from intracellular acidification.

Among all the NMR parameters monitored with RF HT treatment, the TQF ^{23}Na signal levels and the cellular bioenergetic changes measured were the most sensitive to temperature and did not recover after HT. It is unlikely that the late increase in Na_i^+ after HT was caused by an increase in Na^+/H^+ exchanger activity because both pH_i and pH_e returned to the baseline level and the tumour pH_i was neutral ($\sim$7 pH units) after HT. The Na^+/H^+ exchanger has been suggested to be relatively inactive at this pH value [38]. The irreversible increase in Na_i^+ after HT suggests some permanent changes or perhaps damage to the plasma membrane during HT and/or post-HT. The irreversible decrease in NTP/P_i may be due to increased activity of Na^+/K^+ ATPase to maintain the transmembrane Na^+ gradient and/or due to dysfunction of cellular enzymes.

An important issue regarding the application of HT is the spatial uniformity of heating and therapy response throughout the tumour. Although imaging experiments were not performed in the present study, the feasibility of absolute temperature imaging with a paramagnetic thulium complex has recently been demonstrated [32]. The same coil arrangement could be used to image temperature and map the metabolic/physiological responses of tumour during HT treatment; however, such measurements will have poor temporal resolution. Temperature imaging with Tm-complexes requires 3–4 minutes in contrast to only a few seconds for the global tumour temperature measurements by MR spectroscopy techniques. The longer temporal resolution may not be the limiting factor for imaging temperature during HT treatment because the tumours are heated for 60–90 min for the treatment. However, the temporal resolution may not be adequate for controlling the tumour temperature as precisely as achieved in the present study. Similarly, imaging of metabolic and physiological response during HT treatment may be difficult due to longer data collection time compared to the spectroscopy measurements, but imaging measurements can be conducted immediately before and after the treatment to monitor early therapy response.

Acknowledgements

We gratefully acknowledge S.G. Jennings for his helpful discussions and editorial comments. Grant sponsor: NIH grant numbers R33CA110107 and R01EB005964.

Declaration of interest: The authors report no conflicts of interest. The authors alone are responsible for the content and writing of the paper.

References

1. Pennacchioli E, Fiore M, Gronchi A. Hyperthermia as an adjunctive treatment for soft-tissue sarcoma. Expert Rev Anticancer Ther 2009;9:199–210.
2. Hildebrandt B, Wust P. The biologic rationale of hyperthermia. Cancer Treat Res 2007;134:171–184.
3. Falk MH, Issels RD. Hyperthermia in oncology. Int J Hyperthermia 2001;17:1–18.
4. Perez CA, Gillespie B, Pajak T, Hornback NB, Enami B, Rubin P. Quality assurance problems in clinical hyperthermia and their impact on therapeutic outcome: A report by the Radiation Therapy Oncology Group. Int J Radiat Oncol Biol Phys 1989;16:551–558.
5. Bezabeh T, Evelhoch JL, Sloop DJ, Ackerman JJ. Methodology for applied 4 MHz RF hyperthermia concomitant with ^{31}P NMR spectroscopic monitoring of murine tumours. Int J Hyperthermia 2004;20:637–645.
6. Jayasundar R, Hall LD, Bleehen NM. RF coils for combined MR and hyperthermia studies: II. MR coil as a hyperthermic applicator. Magn Reson Imaging 2001;19:117–122.
7. Sreenivasa G, Gellermann J, Rau B, Nadobny J, Schlag P, Deuflhard P, Felix R, Wust P. Clinical use of the hyperthermia treatment planning system HyperPlan to predict effectiveness and toxicity. Int J Radiat Oncol Biol Phys 2003;55:407–419.
8. Babsky A, Hekmatyar SK, Wehrli S, Nelson D, Bansal N. Effects of temperature on intracellular sodium, pH and cellular energy status in RIF-1 tumor cells. NMR Biomed 2004;17:33–42.
9. Babsky A, Hekmatyar SK, Wehrli S, Nelson D, Bansal N. Hyperthermia-induced changes in intracellular sodium, pH and bioenergetic status in perfused RIF-1 tumor cells determined by ^{23}Na and ^{31}P magnetic resonance spectroscopy. Int J Hyperthermia 2005;21:141–158.
10. Mikkelsen RB, Asher CR. Effects of hyperthermia on the membrane potential and Na^+ transport of V79 fibroblasts. J Cell Physiol 1990;144:216–221.
11. Skrandies S, Bremer B, Pilatus U, Mayer A, Neuhaus-Steinmetz U, Rensing L. Heat shock- and ethanol-induced ionic changes in C6 rat glioma cells determined by NMR and fluorescence spectroscopy. Brain Res 1997;746:220–230.
12. Ng TC, Evanochko WT, Hiramoto RN, Ghanta VK, Lilly MB, Lawson AJ, Corbett TH, Durant JR, Glickson JD. ^{31}P NMR spectroscopy of in vivo tumors. J Magn Reson 1982; 49:271–286.
13. Naruse S, Higuchi T, Horikawa Y, Tanaka C, Nakamura K, Hirakawa K. Radiofrequency hyperthermia with successive monitoring of its effects on tumors using NMR spectroscopy. Proc Nat Acad Sci USA 1986;83:8343–8347.
14. Jayasundar R, Honess D, Hall LD, Bleehen NM. Simultaneous evaluation of the effects of RF hyperthermia on the intra- and extracellular tumor pH. Magn Reson Med 2000;43:1–8.

15. Bezabeh T, Evelhoch JL, Thompson P, Sloop DJ, Ackerman JJ. Therapeutic efficacy as predicted by quantitative assessment of murine RIF-1 tumour pH and phosphorous metabolite response during hyperthermia: An in vivo ^{31}P NMR study. Int J Hyperthermia 2004;20:335–357.
16. Hekmatyar SK, Poptani H, Babsky A, Leeper DB, Bansal N. Non-invasive magnetic resonance thermometry using thulium-1,4,7,10-tetraazacyclododecane-1,4,7,10-tetraacetate ($TmDOTA^{-}$). Int J Hyperthermia 2002;18:165–179.
17. Hekmatyar SK, Kerkhoff RM, Pakin SK, Hopewell P, Bansal N. Noninvasive thermometry using hyperfine-shifted MR signals from paramagnetic lanthanide complexes. Int J Hyperthermia 2005;21:561–574.
18. Zuo CS, Mahmood A, Sherry AD. TmDOTA: A sensitive probe for MR thermometry in vivo. J Magn Reson 2001; 151:101–106.
19. Haase A, Frahm J, Hanicke W, Matthaei D. ^{1}H NMR chemical shift selective (CHESS) imaging. Phys Med Biol 1985;30:341–344.
20. Winter PM, Bansal N. Triple-quantum-filtered ^{23}Na NMR spectroscopy of subcutaneously implanted 9L gliosarcoma in the rat in the presence of $TmDOTP^{5-}$. J Magn Reson 2001;152:70–78.
21. Gillies RJ, Liu Z, Bhujwalla Z. 31P-MRS measurements of extracellular pH of tumors using 3-aminopropylphosphonate. Am J Physiol 1994;267:C195–203.
22. Sapareto SA, Dewey WC. Thermal dose determination in cancer therapy. Int J Radiat Oncol Biol Phys 1984; 10:787–800.
23. Kost GJ. pH standardization for phosphorus-31 magnetic resonance heart spectroscopy at different temperatures. Magn Reson Med 1990;14:496–506.
24. Stubbs M, Rodrigues L, Howe FA, Wang J, Jeong KS, Veech RL, Griffiths JR. Metabolic consequences of a reversed pH gradient in rat tumors. Cancer Res 1994;54:4011–4016.
25. ICNIRP 1998 Guidelines for limiting exposure to time-varying electric, magnetic and electromagnetic fields (up to 300 GHz). Health Physics 74;4:494–522.
26. Ettinger KV. Radiofrequency power sources for hyperthermia. In: Field SB, Franconi C, editors. Physics and Technology of Hyperthermia: Dordrecht. M. Nijhoff Publishers, 1987. pp 250–293.
27. Stratton JA. Electromagnetic Theory. York, PA: McGraw-Hill Book Company; 1941.
28. Winter PM, Bansal N. $TmDOTP^{5-}$ as a ^{23}Na shift reagent for the subcutaneously implanted 9L gliosarcoma in rats. Magn Reson Med 2001;45:436–442.
29. Goldsmith M, Damadian R. NMR in cancer. VII. Sodium-23 magnetic resonance of normal and cancerous tissues. Physiol Chem Phys 1975;7:263–269.
30. Damadian R, Cope FW. NMR in cancer. V. Electronic diagnosis of cancer by potassium (39K) nuclear magnetic resonance: Spin signatures and T1 beat patterns. Physiol Chem Phys 1974;6:309–322.
31. De Poorter J, De Wagter C, De Deene Y, et al. Noninvasive MRI thermometry with the proton resonance frequency (PRF) method: In vivo results in human muscle. Magn Reson Med 1995;33:74–81.
32. James JR, Gao Y, Miller MA, Babsky A, Bansal N. Absolute temperature MR imaging with thulium 1,4,7,10-tetraazacyclododecane-1,4,7,10-tetramethyl-1,4,7,10-tetraacetic acid (TmDOTMA(-)). Magn Reson Med 2009;12:12.
33. Hofer KG, Mivechi NF. Tumor cell sensitivity to hyperthermia as a function of extracellular and intracellular pH. J Natl Cancer Inst 1980;65:621–625.
34. Song CW. Effect of local hyperthermia on blood flow and microenvironment: A review. Cancer Res 1984;44: 4721s–4730s.
35. Anderson RL, Hahn GM. Differential effects of hyperthermia on the Na^{+},K^{+}-ATPase of Chinese hamster ovary cells. Radiat Res 1985;102:314–323.
36. Ruifrok A, Kanon B, Konings A. Na^{+}/K^{+} ATPase activity in mouse lung fibroblasts and HeLa S3 cells during and after hyperthermia. Int J Hyperthermia 1986;2:51–59.
37. Lilly MB, Katholi CR, Ng TC. Direct relationship between high-energy phosphate content and blood flow in thermally treated murine tumors. J Natl Cancer Inst 1985;75:885–889.
38. Boyer M, Tannock I. Regulation of intracellular pH in tumor cell lines: Influence of microenvironmental conditions. Cancer Res 1992;52:4441–4447.